Fajardo River Water Resources

Using Earth Observations to Evaluate Land Cover and Water Quality in the Fajardo River Watershed, Puerto Rico

Spring 2025 | California – Ames
April 4th, 2025

Authors: Alex Moran (Analytical Mechanics Associates), Cailan Cumming (Analytical Mechanics Associates), Mel Guo (Analytical Mechanics Associates), Norman Li (Analytical Mechanics Associates)

Abstract: The Fajardo River Watershed, located in Eastern Puerto Rico, drains into vulnerable coastal areas that contain critical marine ecosystems like coral reefs, seagrass beds, and mangrove forests. Assessments of land and water health in the region have been limited, and the impacts of land-based pollution on surrounding marine areas are unclear. DEVELOP partnered with two Puerto Rico-based, marine conservation groups—Sociedad Ambiente Marino (SAM) and the Environmental Mapping Consultants (EMC)—and collaborated with NASA's Water2Coasts project to examine the viability of remote sensing to assess land cover land use change (LCLUC) and coastal water quality in the region. Using data from Landsat 7 Enhanced Thematic Mapper Plus (ETM+), Landsat 8 Operational Land Imager (OLI), Envisat Medium Resolution Imaging Spectrometer (MERIS), Suomi National Polar-Orbiting Partnership (NPP) Visible Infrared Imaging Radiometer Suite (VIIRS), and Plankton, Aerosol, Cloud, ocean Ecosystem (PACE) Ocean Color Instrument (OCI) satellites, our LCLUC analysis found increased vegetation cover and decreased crop and barren land cover over the past two decades. Our water quality analysis indicated moderate concentrations of chlorophyll-*a* and K_d490—two important water quality indicators—and observed higher concentrations during Puerto Rico's rainy seasons. We were unable to evaluate the relationship between LCLUC and coastal water quality due to coarse data resolution and limits in data availability. However, by analyzing regional water quality trends, we were able to inform our partners' decision-making processes in coral reef conservation and assist in the identification of at-risk coral reef sites and locations of potential water quality monitoring stations. We determined that Earth observations successfully reflected local observations and can be utilized by partners for more advanced assessments of ocean and land health in the area.

Key Terms: remote sensing, LCLUC, water quality, chlorophyll-*a*, K_d490, Landsat, MERIS, PACE

Advisors: Dr. Morgan Gilmour (NASA Ames Research Center), Dr. Juan Torres-Pérez (NASA Ames Research Center)

Lead: Lauren Webster (California – Ames)

1. Introduction

1.1 Background Information & Scientific Basis

Coastal and marine ecosystems have degraded worldwide due to changes in land cover and land uses that pollute coastal waters (Locke, 2024). Among these ecosystems, coral reefs are one of the most biodiverse yet highly threatened, with up to 67% of their historical global extent lost (Good et al., 2021; Devlin, 2022). The coral reefs remaining today face a variety of stressors, including warming ocean temperatures, ocean acidification, overfishing, and land-based pollution. Of the local pressures to coral reefs, land-based pollution is particularly concerning, as it introduces excessive nutrients, sediments, and contaminants into coastal waters (Ramos-Scharron et al., 2014).

One such area that has experienced land-based pollution is the Fajardo River watershed (FRW), a 69 km^2 region in northeastern Puerto Rico that drains into coral reefs, mangrove forests, and seagrass beds in the Vieques Sound and Northeast Marine Corridor (Figure 1). In the past few decades, the FRW has experienced significant land cover land use change (LCLUC) and local community members have expressed concerns about LCLUC affecting their communities and coastal ecosystems. These changes have resulted from agricultural runoff, overgrazing, sanitary sewage discharge, poorly maintained roads, and vegetation removal practices (Protectores de Cuencas, 2017). Furthermore, intense hurricanes (e.g. Hurricane María) in the past decade have severely altered the land cover, utility infrastructure, and hydrology of the watershed. Additionally, these hurricanes and extreme rains events introduce ecosystem stressors—uprooting coastal flora, increasing sediment in coastal waters, and damaging coral reef structures—that adversely impact aquatic life (recently summarized by Locke, 2024).

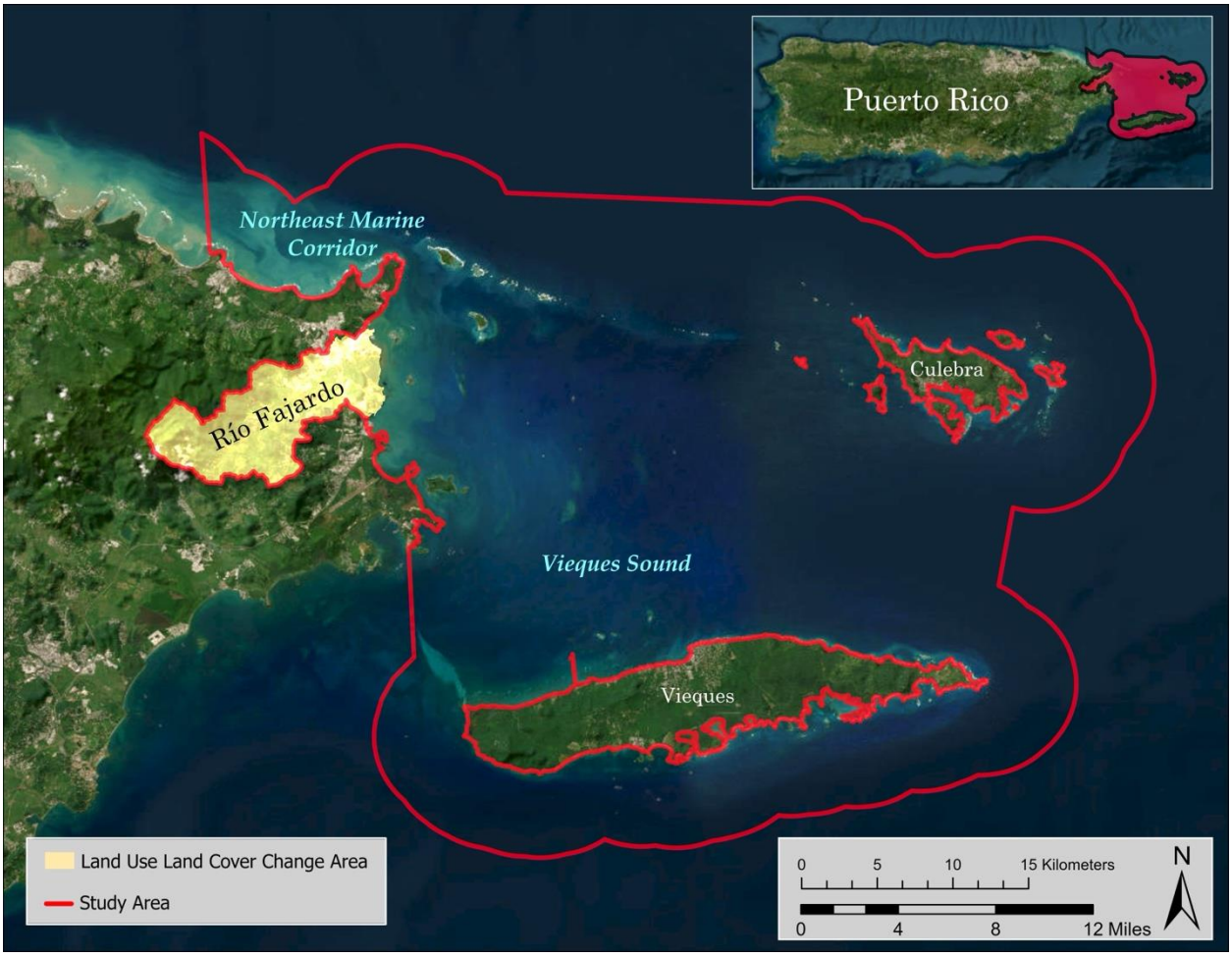

Figure 1. Study area of the Fajardo River watershed and Northeast Marine Corridor, including the coastal and marine areas of the Vieques Sound. (Data Source: USGS, ESRI, Earthstar Geographics, 2025).

This project studied LCLUC in the FRW alongside water quality, as LCLUC can determine the types and quantities, as well as speed and pathways of pollutants that can be transported into water bodies (Saeidi et al., 2023). A large body of research highlights the impacts of runoff development and soil erosion on water quality and aquatic ecosystem health (Locke, 2024). Notably, runoff may introduce excess sediment, nutrients, and pollution, reducing light availability and restricting aquatic photosynthesis in reef environments (Locke, 2024). Several kilometers offshore from the FRW outlet, in the Arrecifes de La Cordillera Natural Reserve, scientists have documented a decrease in living coral cover and fish assemblages since the late 1990s and interpreted that the decline resulted from poor water quality pulses from the FRW, among other pressures (Ramos-Scharron et al., 2014). To investigate the potential for continued impacts in that region and beyond, this project evaluated water quality from 2002–2025 in the Vieques Sound, which encompasses the coastal and marine areas of northeastern Puerto Rico, Culebra Island, and Vieques Island.

Since the 1970s, satellite remote sensing data has been utilized for land use and water resource management. Remote sensing imagery enables spatially and temporally detailed assessments of LCLUC across large regions (Zhu et al., 2022), and scholars have used it to analyze principal trends in LCLUC in eastern Puerto Rico from the 1930s to the early 2000s (Ramos-Scharron et al., 2014; Zhu et al., 2022). Since the 1990s, remote sensing has also been an effective tool for deriving water quality parameters in oceans (Warren et al., 2021). This project focused specifically on chlorophyll-*a* concentrations and turbidity (represented by K_d490), as

they indicate the health of water bodies (Warren et al., 2021) and critically inform the ecosystem function of coral reefs (Otero & Carbery, 2005).

1.2 Project Partners and Project Objectives

To support protection efforts of water quality in Puerto Rico's coastal and marine habitats, we partnered with two Puerto Rico-based organizations, Sociedad Ambiente Marino (SAM) and Environmental Mapping Consultants (EMC). SAM is a community-based environmental organization that promotes coastal resilience through marine rehabilitation, conservation, scientific research, and education. EMC addresses challenges in coastal and marine ecosystems through integration of remote sensing technology, geographic information systems, and field surveys. To support the partners' decision-making, this project utilized Earth observations to evaluate if there was a relationship between LCLUC and coastal and marine water quality in northeastern Puerto Rico. Our team produced and analyzed LCLUC maps of the FRW and maps of chlorophyll-*a* concentrations and turbidity in the Vieques Sound from 2002 to 2025. Since January 2025, EMC has been collecting in situ water quality measurements between Puerto Rico's northeastern coast and Culebra Island. The maps generated by this project aimed to provide a more widespread assessment of water quality throughout the Vieques Sound, which can support EMC's determination of future water monitoring stations and assist SAM in assessing its coral reef aquaculture and restoration sites. Additionally, these maps can support partner efforts in guiding watershed management priorities and educating coastal communities.

2. Methodology

2.1 Data Acquisition

Our study of LCLUC and marine water quality leveraged a mixture of Earth observations and in situ data (Table 1). To conduct a decadal analysis of LCLUC from 2000 to 2024, we utilized data from the Landsat missions, which are jointly managed by NASA and the U.S. Geological Survey (USGS). From the USGS Earth Explorer data portal, we acquired Collection 2 Level-2 Surface Reflectance data from Landsat 7 Enhanced Thematic Mapper Plus (ETM+) and Landsat 8 Operational Land Imager (OLI). Within USGS Earth Explorer, we filtered Landsat imagery to <10% cloud cover for the desired region and time frame of the study.

Table 1. *Data used to measure LCLUC and water quality*

Platform & Sensor	Products	Provider	Spatial Resolution	Dates
Landsat 7 ETM+	Collection 2 Level-2 Surface Reflectance	NASA/USGS	30 m	Mar – May 2000
Landsat 8 OLI	Collection 2 Level-2 Surface Reflectance	NASA/USGS	30 m	Oct – Dec 2014; Oct – Oct 2024
Envisat MERIS	ENVISAT MERIS Level-3 Mapped Chlorophyll, Version 2022	NASA	4 km	Oct 2002 – Apr 2012
	ENVISAT MERIS Level-3 Mapped Downwelling Diffuse Attenuation Coefficient, Version 2022	NASA	4 km	Oct 2002 – Apr 2012
Suomi NPP VIIRS	SUOMI-NPP VIIRS Level-3 Mapped Chlorophyll, Version 2022	NASA	4 km	Feb 2012 – Jan 2025
	SUOMI-NPP VIIRS Level-3 Mapped Downwelling Diffuse Attenuation Coefficient, Version 2022	NASA	4 km	Feb 2012 – Jan 2025

PACE OCI	Provisional PACE OCI Level-3 Mapped Chlorophyll, Version 3.0	NASA	4 km	Apr 2024 – Jan 2025
	Provisional PACE OCI Level-3 Mapped Downwelling Diffuse Attenuation Coefficient, Version 3.0	NASA	4 km	Apr 2024 – Jan 2025
Rio Fajardo NR FAJARDO, PR -50071000 site data	Monthly River Discharge Data	USGS	0 m	Jan 2002 – Jan 2024
EMC Monitoring Stations	Chlorophyll concentration	Environmental Mapping Consultants	0 m	Jan 2025

To evaluate marine water quality, we collected Level-3 data from Envisat Medium Resolution Imaging Spectrometer (MERIS), Suomi National Polar-orbiting Partnership Visible Infrared Imaging Ratiometer Suite (Suomi NPP VIIRS), and the Plankton, Aerosol, Cloud, and ocean Ecosystem Ocean Color Instrument (PACE OCI) from NASA's Ocean Color Database as NetCDF files. The satellite data collected included preprocessed K_d490 and chlorophyll-*a* data for our study area. Our partner, EMC, provided in situ water quality data from seven monitoring stations along the Fajardo coastline to help evaluate the accuracy of PACE OCI data from January 2025. Lastly, we obtained Fajardo River discharge data from USGS.

2.2 Land Cover Data Processing

After downloading Landsat Collection 2 Level-2 Surface Reflectance data from USGS Earth Explorer, we conducted cloud removal and correction in ArcGIS Pro (v3.3.0). This process involved utilizing the Landsat Collection 2 Level-2 Quality Assessment (QA) band as the reference cloud mask to remove clouds from the imagery. To replace the missing data from cloud cover with imagery from another date, we conducted cloud removal and correction on the other imagery and mosaicked the collective imagery to form a mostly cloud-free image. We conducted this process for Landsat 7 ETM+ imagery in 2000 and Landsat 8 OLI imagery in 2014 and 2024 to prepare for decadal analysis of LCLUC.

Following cloud removal and correction, we ran an unsupervised classification algorithm, K-means clustering in Python (v3.10.16), to identify spectral patterns across the study area and help establish boundaries of land cover types (Table 2). We referenced the K-means clustering results alongside the classification scheme from NOAA's C-CAP 2010 30 Meter Land Cover product of Puerto Rico to design the LCLUC classification scheme for this project.

Table 2. *Visualization of the LCULC classes chosen.*

Land Cover Type	Description
Developed areas	Land that is primarily covered by concrete, asphalt, and other constructed materials
Woody Vegetation	Forested areas mainly covered by trees
Water	Areas of open water with minimal vegetation or soil cover
Shrubland	Areas dominated by shrubs, young trees in early successional stage, or stunted trees

Herbaceous/Pasture	Land that is primarily covered by grasses and herbaceous vegetation and can be utilized for grazing
Cropland	Land that is devoted to production of annual crops, including hay production and areas being actively tilled.
Barren Ground	Bare and dry areas with minimal vegetation

2.3 Water Quality Data Processing

We used preprocessed Level-3 satellite data from NASA's Ocean Biology Processing Group (OBPG). We leveraged precalculated K_d490 data from OBPG's standard algorithm (Werdell et al., 2024) for the diffuse attenuation coefficient for downwelling irradiance at 490 nm. The chlorophyll-*a* calculation uses OBPG's standard chlorophyll algorithm (O'Reilly et al., 2023) and includes additional quality control flags to ensure at least 50 percent of the pixels used in the calculation of chlorophyll-*a* are valid. Examples of invalid pixels included data flagged as land, straylight and high glint. These files were then converted to CSV format and raster datasets to conduct data analysis.

Working with USGS discharge data, we removed data containing missing monthly average measures for sediment concentration and sediment volume and removed dates containing missing data from our analysis. We used Python (v3.12.8) to filter USGS discharge volume data to our study period. No further processing was needed as USGS provides continuous, uninterrupted monthly averages starting in 1983. Lastly, we removed negative values from the in-situ water quality measurements and replaced negative measurement with zero for our analysis.

2.4 Land Cover Data Analysis

We calculated EVI and added it as a feature to our classification mode to enhance model sensitivity to dense vegetation in Puerto Rico's tropical environment (Vijith & Dodge-Wan, 2020). EVI corrects for some atmospheric conditions and canopy background noise, making it more sensitive to high biomass conditions.

Equation 1 calculates Enhanced Vegetation Index (EVI) which includes near-infrared (NIR), red (R), and blue (B) spectral bands. G is the gain factor of 2.5, C_1 and C_2 are coefficients for atmospheric correction, the L value adjusts for canopy background noise (Huete et al., 2002).

$$EVI = G \cdot \left(\frac{(NIR - R)}{(NIR + C1 \cdot R - C2 \cdot B + L)} \right) \qquad (Equation\ 1)$$

To prepare for supervised classification of land cover, we generated at least 150 training data points for each land cover class in ArcGIS Pro. This process involved visually interpreting the land cover types of training data points in 2024 Landsat 8 OLI data by referencing high-resolution imagery from Google Earth Pro (v7.3.6) within our study area and timeframe. To ensure the quality of our training data, we validated the land cover types of specific sites with in-situ knowledge from our Puerto Rico-based partners.

We trained various pixel-based supervised classification models in Python and utilized the best performing model to generate LCLUC maps. To start, we randomly allocated 70% of point data for model training and 30% of point data for model testing. Then we trained a Support Vector Machine (SVM), Random Forest (RF), and Decision Tree (DT) model on the 2024 Landsat 8 OLI composite image. The RF model with 450 trees performed the best, and we assessed its performance using several metrics: overall accuracy, precision, recall, and F-1 score. We proceeded to apply our best-performing RF model to generate land cover land use maps from 2000 Landsat 7 ETM+ imagery and 2014 and 2024 Landsat 8 OLI imagery. We conducted a decadal time series as it was determined that LCLUC analysis within a shorter timeframe would not be meaningful to our partners.

2.5 Water Quality Data Analysis

For each satellite's data (Table 1), we extracted K_d490 and chlorophyll-*a* values from the study period using Python (v.3.12.8) and ArcGIS Pro (v3.3.0). We divided the extracted data among three subregions—a 3km buffer around the Fajardo Coast, the Northeast Ecological Corridor Coastline, and the Vieques Sound—to conduct more comprehensive data processing and analysis of the study area. Based on the preprocessing of the data, we used each raster cell's center coordinates for its geographic positioning within the study area. Next, we calculated the mean monthly K_d490 and chlorophyll-*a* levels for each subregion. With the MERIS and VIIRS data, we created four time series plots comparing the mean monthly K_d490 and chlorophyll-*a* values of the three subregions between January 2002 to April 2012 and February 2012 to January 2025.

For PACE OCI data, we created two monthly line plots from April 2024 to January 2025 through SeaBorn's (v0.13.2) statistical data visualization Python library. These graphs reflect the monthly K_d490 and chlorophyll-*a* levels from the same area of the Fajardo Coastline as the EMC's monitoring stations and highlight the yearly trends of both metrics. Additionally, we assessed the quality of the PACE OCI remote sensing data by comparing our partner's mean in situ measurements from January 26, 2025, with the satellite data collected, plotting points from both datasets on the same graph.

We then created two geospatial maps to reflect the K_d490 and chlorophyll-*a* concentrations over the study area for November 2024. Using the NetCDF files for both datasets, we clipped and resampled the raster layers that were created in ArcGIS Pro (v3.3.0). A bathymetric seabed model was added, along with land flowlines and coral reef areas from the USGS hydrography dataset for Puerto Rico to create the final spatial visualizations. The original rasters, along with the visual aids created by the resampled data, helped identify areas with higher turbidity and chlorophyll-*a,* as well as potential areas for future monitoring.

Finally, we created a seasonality plot using the mean monthly discharge data. This process involved taking the mean for four seasons—January to March, April to June, July to September, and October to December—to analyze seasonal river discharge trends. We then plotted the mean monthly K_d490 data for the Fajardo coastline between 2002 and 2012. We graphed both seasonality plots onto a single graph to compare seasonal discharge and turbidity trends.

3. Results

3.1 Land Cover Analysis of Results

The RF model achieved an overall accuracy of 72% with varying levels of performance across the 7 land cover classes (Table 3). The model achieved the highest F1-scores for classifying water (0.93), barren ground (0.88), developed areas (0.87), and woody vegetation (0.76). However, our F1-scores showed that it was more difficult to accurately classify herbaceous land or pasture (0.62), shrubland (0.50), and cropland (0.50). These 3 land cover types are more difficult to classify due to spectral similarities between their landscapes. Both shrubland and cropland areas contain significant herbaceous cover. Additionally, the boundaries between these classes can be ambiguous since unmanaged cropland or pastures are often undergoing ecological succession and transitioning into shrubland.

Table 3. *Random forest model's performance metrics across the 7 land cover types.*

	Precision	Recall	F1-Score	Support
Developed Areas	0.91	0.82	0.87	51
Woody Vegetation	0.76	0.75	0.76	52
Water	0.93	0.93	0.93	45
Shrubland	0.47	0.54	0.50	52
Herbaceous/Pasture	0.61	0.64	0.62	53
Cropland	0.56	0.45	0.50	53
Barren Ground	0.83	0.93	0.88	54

The classification model generated three LCLUC maps from Landsat imagery for the years 2000, 2014, and 2024 (Figures 2–4). The classification map from 2000 was derived from Landsat 7 ETM+ imagery, and our classification maps from 2014 and 2024 were derived from Landsat 8 imagery. From 2000 to 2024, the classification showed developed areas dominating in the northeast near the mouth of the Fajardo River. Spanning from the northeast to the southwest, the central strip of the watershed was a mosaic of land cover and uses that morphed through the years. El Yunque National Forest resides in the western end of the watershed, and woody vegetation consistently covered this region during the study period. Missing data from cloud removal was a consistent feature of this forested area since it received year-round cloud cover and rainfall.

The 2000 classification showed that the central strip of the watershed was predominantly a mixture of cropland and barren ground, with some herbaceous land and shrubland (Figure 2). However, this classification is uncertain due to the model's lowered performance in classifying shrubland, herbaceous land, and cropland. Along the eastern coast, the mangrove forest, Bosque de Ceiba, was misclassified as a water body likely due to sensor differences between Landsat 7 ETM+ and Landsat 8 OLI.

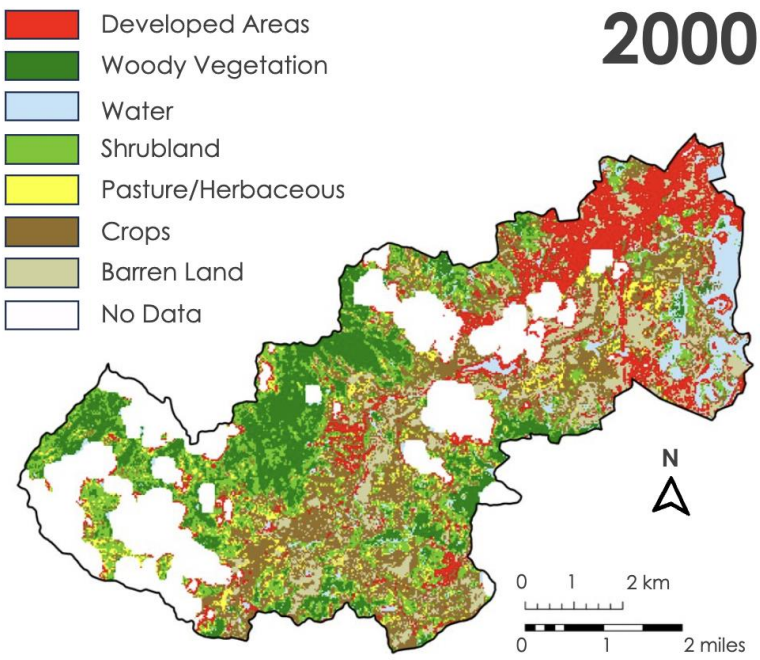

Figure 2 LCLUC map of the Fajardo River watershed in 2000 across 7 land cover types.

The 2014 classification indicated that much of the cropland and barren ground from 2000 had transformed into shrubland and herbaceous land (Figure 3). In the eastern end of the watershed, our map also showed a new developed area east of Highway 53 (Figure 3).

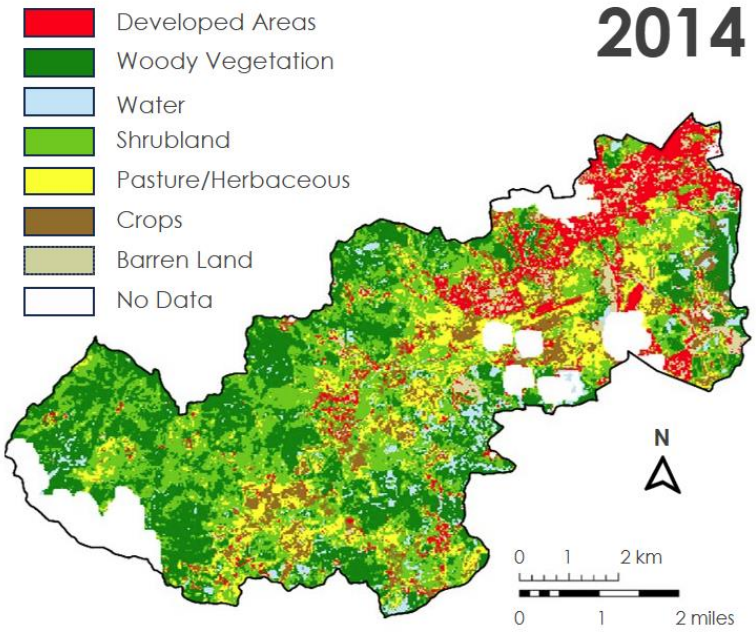

Figure 3. LCLUC map of the Fajardo River watershed in 2014 across 7 land cover types.

The 2024 classification illustrated a significant increase in overall natural vegetation. Cropland continued to convert into either herbaceous land or shrubland, and much of the shrubland had transformed into woody vegetation. Compared to 2014, the coverage of developed areas in 2024 also appeared more homogenous and less mixed with barren ground (Figure 4).

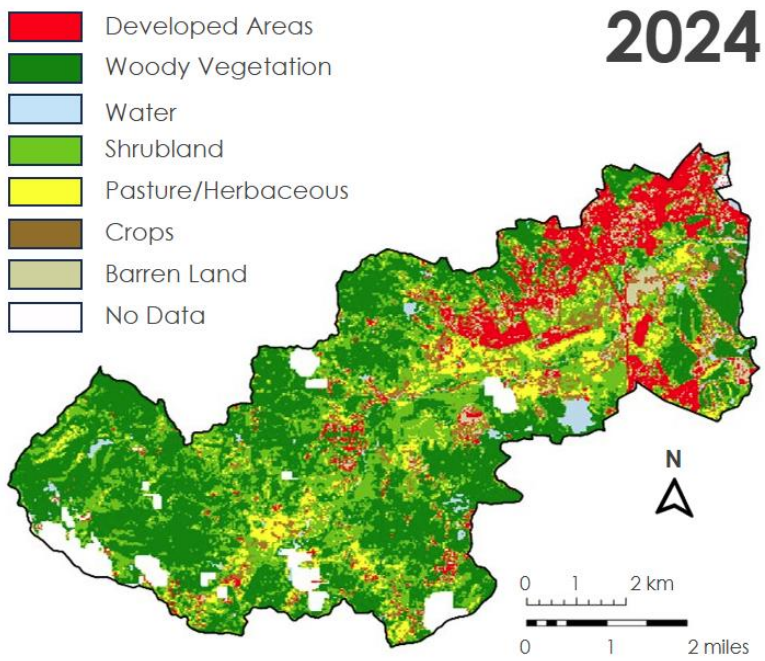

Figure 4. LCLUC map of the Fajardo River watershed in 2024 across 7 land cover types.

3.2 Water Quality Analysis of Results

Using MERIS and Fajardo River discharge between 2002 and 2012, we created seasonality time series chart to compare mean K_d490 values for the Fajardo River coastline with monthly, mean discharge volumes measured in cubic feet per second. We observed a potential relationship between seasonal discharge rates and an increase in turbidity along the Fajardo Coast (Figure 5). We observed an increase in K_d490 and chlorophyll-*a* concentrations between the months of August to November. This cyclical pattern follows the rainy period for Puerto Rico and the Caribbean, however we are unable to draw conclusions on the impacts of discharge on coastal turbidity given the multiple external factors, such as precipitation, that may be contributing to both measurements.

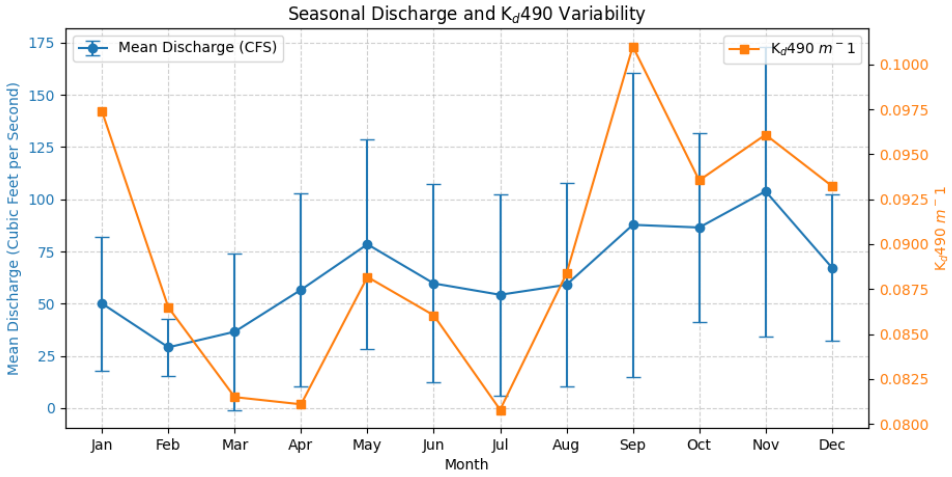

Figure 5. Chart of Fajardo River coastline K_d490 and Fajardo River discharge seasonal trends.

Examining all chlorophyll-*a* for all three subregions between 2002 to 2012 we observed a similar cyclical trend seen with K_d490, with increased concertation of chlorophyll-*a* reaching their peaks between the months of August and November (Figure 6). These results indicate the potential for chlorophyll-*a* to be a measurable contributor to the observed turbidity increases within the study area. Additionally, this trend aligns with previous research that demonstrates a positive relationship between rain and turbid water quality (Seers & Shears, 2015). Notably, in Figure 6, we observed a significant chlorophyll-*a* increase in September 2004 coinciding with Hurricane Jeanne which impacted the island on September 14, 2004, highlighting the relationship between tropical storms and water quality metrics. Additionally, in Figure 6, we observe a downward K_d490 concentrations along the Fajardo River coastline between 2002 to 2012 however, the results in Table A1 show this trend is not statistically significant.

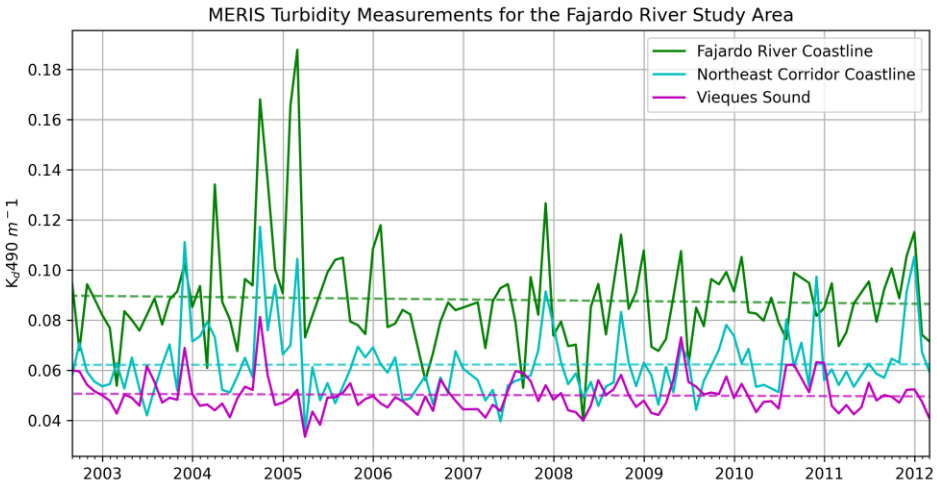

Figure 6. Chart of K_d490 for the three subregions between 2002 to 2012.

We then analyzed these two water quality metrics between 2012 and 2024 with Suomi NPP VIIRS and observed a similar cycle pattern, with both metrics being within expected concentration levels for their respective marine sub-regions. Plotting trendlines for both water quality metrics, we observe a positive, upward trends for the Fajardo River coastline; however, looking at Table A2, we observe that the relationships is not a statistically significant relationship with a P-Value of ~0.628.

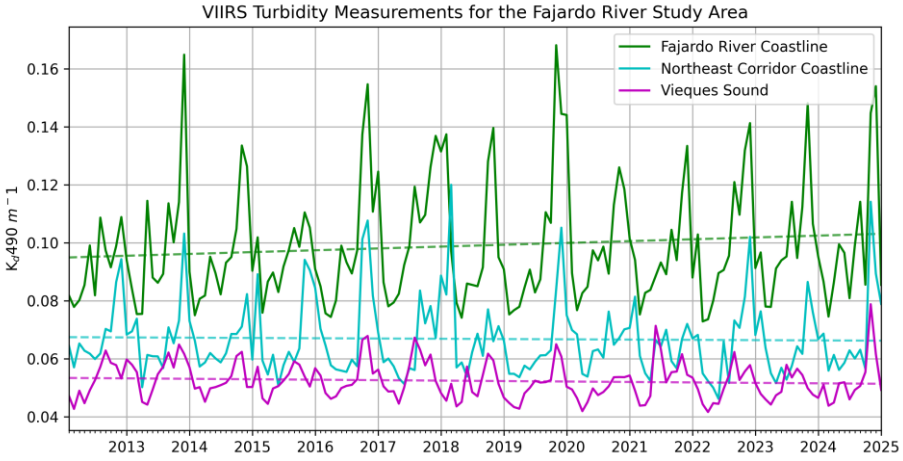

Figure 7. K_d490 levels for the three subregions between 2012 to 2024.

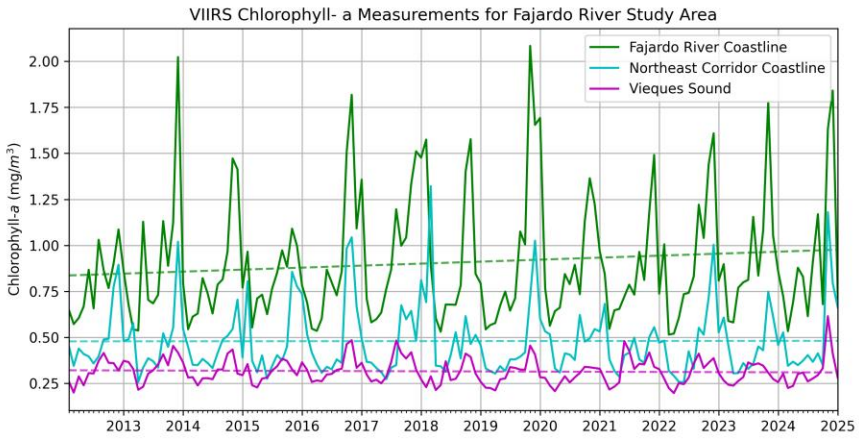

Figure 8. Chlorophyll-*a* for the three subregions between 2012 to 2024.

In graphing the PACEOCI mean monthly K_d490 and chlorophyll-*a* measurements between April 2024 and January 2025 along the Fajardo coastline, where the highest concentrations of both parameters were found, we observed a similar range of moderate levels of chlorophyll-*a* and K_d490 as that of previous years — years which recorded ranges of 0.04 – 0.20 K_d490 (m^{-1}) and 0.25 – 3.5 chlorophyll-*a* (mg m^{-3}; Seers & Shears, 2015; Shi & Wang, 2010). We observed a similar cyclical pattern as previous years where K_d490 and chlorophyll-*a* levels appeared to increase with higher levels of recorded precipitation in the region, with the highest concentrations of turbidity measured in November and December of 2024 (Figure *9*).

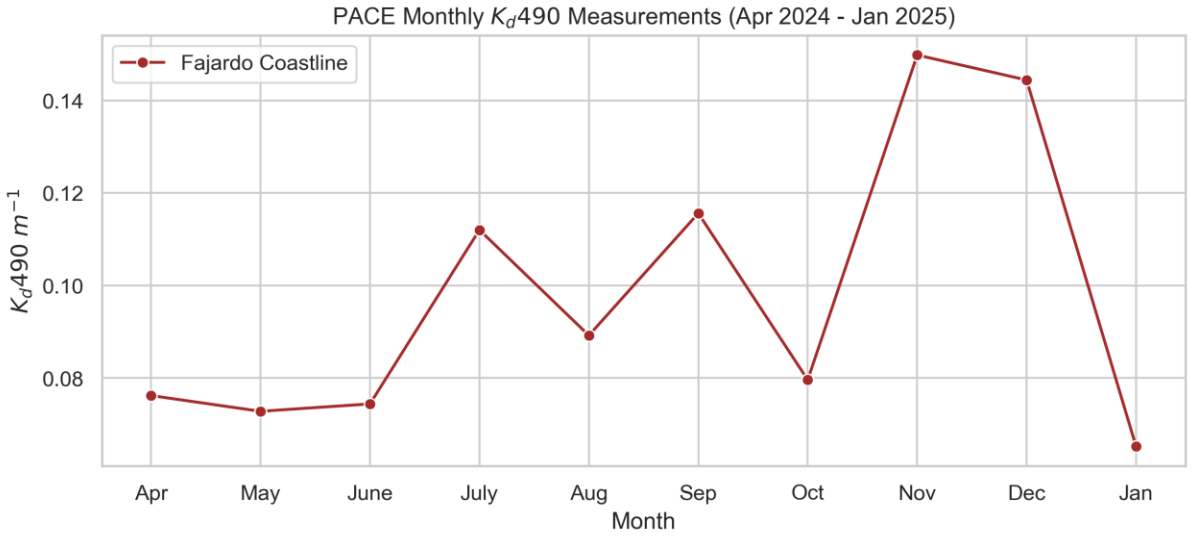

Figure 9. K_d490 in the Fajardo coastline between April 2024 and January 2025.

We were not able to directly compare the remote sensing data to the in situ chlorophyll-*a* measurements taken by EMC on January 26, 2025 due to PACE's lower resolution data (Figure 10). However, we concluded that the PACE satellite returned data that was within the expected range of measurements based on historical trends and local observations.

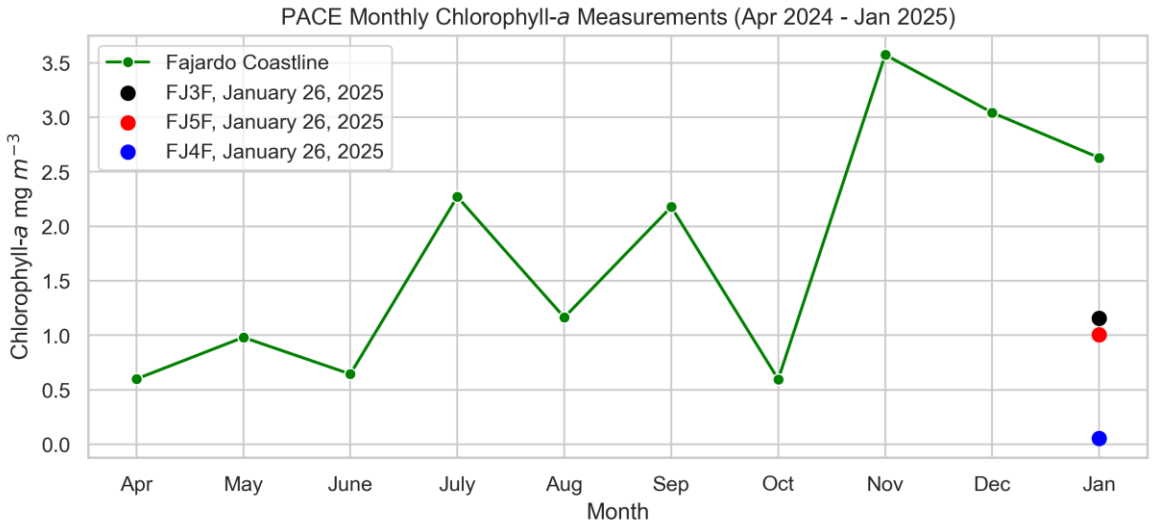

Figure 10. Chlorophyll-*a* in the Fajardo coastline between April 2024 and January 2025.

We mapped the K_d490 and chlorophyll-*a* monthly concentrations in November 2024 the month with the highest recorded levels between April 2024 and January 2025 (Figures 11 and 12). We were able to identify and communicate the areas with the highest levels of K_d490 and chlorophyll-*a*: the Fajardo Coast, Northeast Ecological Corridor, and West Coast of Vieques island. These levelswere still within the moderate range described above. . We observed lower K_d490 and chlorophyll-*a* levels near Culebra Island compared to the higher concentration areas, though the coast of Culebra did experience higher average levels than surrounding open ocean areas. We also identified that many critical ecosystems, particularly coral reef habitats, are located in areas with higher concentrations of both water quality metrics.

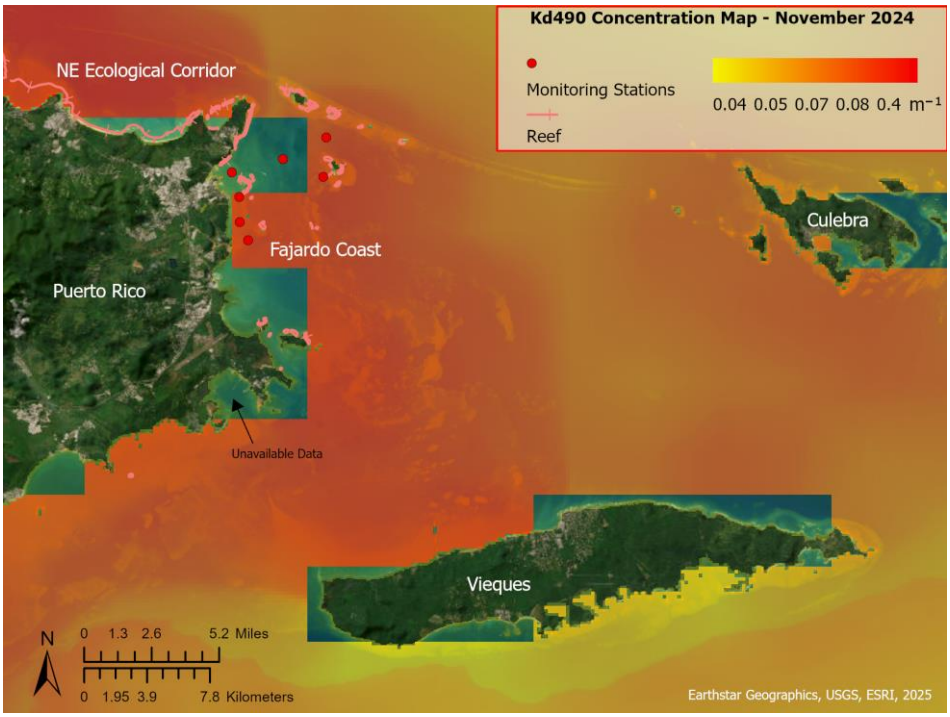

Figure 11. Map of K_d490 levels in November 2024.

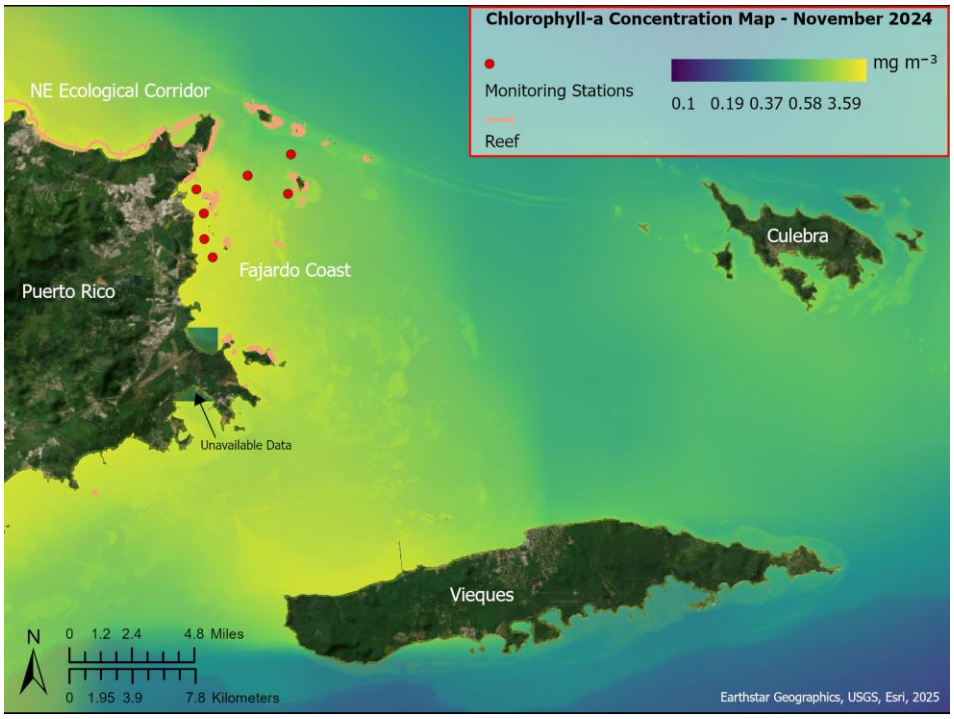

Figure 12. Map of chlorophyll-*a* levels in November 2024.

3.3 Errors & Uncertainties

We encountered several limitations in conducting the LCLUC analysis, particularly in the classification map for the year 2000. The Random Forest model was trained on Landsat 8 OLI imagery; however, the 2000 classification map was derived from Landsat 7 ETM+ imagery. There are a few key differences between the surface reflectance data from Landsat 7 and Landsat 8, particularly in the wavelength range of the near-infrared and shortwave infrared bands. These bands help indicate vegetation and water content, so the classification of natural and cultivated vegetation was erroneous in 2000. For instance, a mangrove forest was misclassified as water that year, likely due to the high-water content in mangroves. The 2000 classification of significant cropland and barren ground coverage is also uncertain since the National Land Cover Database (NLCD) 2001 of Puerto Rico classified much of this area to be either herbaceous land or pasture. Missing data from cloud coverage was also an uncertainty in the LCLUC analysis. Given our small tropical study area, cloud coverage was consistent through the years and complicated the process of image acquisition.

Additionally, discrepancies between remote sensing datasets of varying spatial and spectral resolutions introduced inherent uncertainties. The algorithms used to derive K_d490 and chlorophyll-*a* products also create uncertainty over land pixels that could be incorrectly flagged or could introduce contamination from mixed pixels. Validation efforts were further constrained by the limited temporal coverage of our partner's in-situ data, as collection only began a week prior to the project start, leaving minimal overlap for effective comparison with Earth observation data. Moreover, the coarse resolution for level 3 Envisat MERIS, Suomi NPP VIIRS, and PACE OCI products presents limitations in capturing more localized turbidity results along the Fajardo coast.

4. Conclusions

4.1 Interpretation of Results

We found that Earth observations alone are insufficient to evaluate the potential relationship between LCLUC and marine water quality in northeastern Puerto Rico. However, our results can independently provide a decadal understanding of LCLUC and marine water quality trends since 2000. The LCLUC results indicated an overall decrease in cropland and barren ground along with an increase in woody vegetation cover

and shrubland. Our classification also showed the coverage of developed areas to be more homogenous by 2024, which indicates a potential increase in impervious surfaces and urban density.
We observed that all reported K_d490 and chlorophyll-*a* levels across the marine subregions follow a cyclical trend throughout our study period that coincides with water discharge and the rainy season. Overall, all marine subregions' water quality parameters were within expected moderate ranges given their locations—with areas closer to the coastline seeing higher levels of both water quality metrics—throughout the study period. While we observed slight upward trends for both water quality metrics along the Fajardo River coastline between 2012 to 2024, the results were not statistically significant, indicating that K_d490 and chlorophyll-*a* level ranges have stayed relatively consistent within the past two decades. Due to similar trends in K_d490 and chlorophyll-*a*, algae may be a main contributor to the turbidity levels reflected by the K_d490 measurements, but further research would be needed to evaluate the exact variables influencing turbidity and whether it lowers overall water quality.

4.2 Feasibility & Partner Implementation

Based on our results, we determined that it is feasible to use PACE satellite data to evaluate water quality in eastern Puerto Rico, with some limitations. While it was feasible to evaluate levels of K_d490 and chlorophyll-*a* with remote sensing data–two key parameters in determining water quality–it was infeasible to determine whether higher concentrations necessarily result in poorer water quality in the area. However, partners will be able to utilize the project methodology to do more advanced assessments of ocean health with the PACE satellite as more data becomes available and new data products are released. Because of the hyperspectral capabilities of PACE OCI, partners may be able to better determine the composition of phytoplankton communities in the area and determine whether these communities are harmful or non-harmful to local ecosystems and overall water quality. We determined that it is not feasible to conduct direct comparisons between remote sensing data from PACE and current in situ measurements based on its low resolution. Even with this limitation, our results give partners an accurate baseline of the most current water quality information available, and an understanding of historical trends that can help inform conservation and restoration efforts in the future, such as the identification of areas for future monitoring sites and areas in which critical ecosystems could be negatively impacted by higher levels of turbidity.

We also determined that it was not feasible to draw a direct relationship between land cover land use change in the Fajardo River Watershed and water quality in the connected coastal areas due to the fact that a variety of influencing factors not included in LCLUC in the watershed, such as natural coastal erosion, could impact coastal water quality.

5. Acknowledgements

The Fajardo River Water Resources team would like to thank the following people for their contributions to and support of our project:

Partners and Collaborators: Dr. William Hernández, Dr. Roy Armstrong — Environmental Mapping Consultants | Samuel Suleimán, Dr. Edwin A. Hernández-Delgado — Sociedad Ambiente Marino | Dr. Carlos Ramos-Scharrón — NASA Water2Coasts

Science Advisors: Dr. Morgan Gilmour, Dr. Juan Torres-Pérez, Dr. Liane Guild — NASA Ames Research Center

NASA DEVELOP Leads & Fellow: Lauren Webster, Katie Miller, Maya Hall — California – Ames

NASA DEVELOP National Program Office: Sarah Hafer-Martin

Thank you to Savannah Cooley, Milan Loiacono, and NASA Earth Exchange scientists Dr. Kyle Kabasares, Dr. Keiko Nomura, and Dr. Conor Doherty.

This material contains modified Envisat MERIS data (2002-2014), processed by ESA.

Any opinions, findings, and conclusions or recommendations expressed in this material are those of the author(s) and do not necessarily reflect the views of the National Aeronautics and Space Administration.

This material is based upon work supported by NASA through contract 80LARC23FA024.

6. Glossary

- **ArcGIS** – Geographic Information System software provided by Esri
- **Chlorophyll-*a*** – Pigment found in plants and algae, commonly used to measure the amount of algae growing in a waterbody
- **Decision Tree** – Non-parametric supervised learning algorithm used for both classification and regression
- **Earth observations** – Satellites and sensors that collect information about the Earth's physical, chemical, and biological systems over space and time
- **EMC** – Environmental Mapping Consultants
- **ENVISAT** – "Environmental Satellite", part of the ESA's fleet of earth observing satellites, decommissioned in 2012
- **ESA** – European Space Agency
- **ETM+** – Enhanced Thematic Mapper Plus
- **EVI** – Enhanced Vegetation Index, helps quantify vegetation greenness, particularly in dense vegetation areas
- **In-Situ Data** – Data collected in the original place/position.
- **K_d490** – Diffuse attenuation coefficient at 490 nm, representing the rate at which light is attenuated with depth, and often used as a proxy for water turbidity
- **Landsat** – A series of Earth-observing satellites jointly managed by NASA and USGS
- **LCLUC** – Land cover land use change **–** classification of land based on environmental characteristics (land cover) or human activities (land use), their change over time
- **MERIS** – Medium Resolution Imaging Spectrometer
- **NASA** – National Aeronautics and Space Administration
- **NetCDF** – A multidimensional file format

- **NLCD** – National Land Cover Database
- **NOAA** – National Oceanic and Atmospheric Administration
- **OCI** – Ocean Color Instrument
- **OLI** – Operational Land Imager
- **PACE** – Plankton, Aerosol, Cloud, ocean Ecosystem mission
- **Random forest** – Machine learning algorithm that uses an ensemble of decision trees, commonly used for classification or regression
- **Raster** – A fundamental data structure consisting of a matrix of equally sized cells representing a location on the earth's surface and contains a numeric value that represents a particular attribute
- **Remote Sensing** – Process of collecting information about an object without physically contacting it, in this context collecting information with satellites
- **SAM** – Marine Environment Society, Spanish acronym: Sociedad Ambiente Marino
- **Suomi NPP** – Suomi National Polar-orbiting Partnership
- **Support Vector Machine** – Supervised machine learning algorithm used for classification and regression tasks
- **Time Series** – set of data collected or calculated over intervals of time
- **Turbidity** – measure of the cloudiness or haziness of water caused by suspended particles and organic matter that reduce light penetration
- **USGS** – U.S. Geological Survey
- **VIIRS** – Visible Infrared Imaging Radiometer Suite

7. References

Devlin, M. J. (2022). Coral reefs: The good and not so good news with future bright and dark spots for coral reefs through climate change. *Global Change Biology*, 28(15), 4506–4508. https://doi.org/10.1111/gcb.16271

Earth Resources Observation and Science (EROS) Center. (2020). *Landsat 8-9 Operational Land Imager / Thermal Infrared Sensor Level-2, Collection 2 Surface Reflectance*. U.S. Geological Survey. https://doi.org/10.5066/P9OGBGM6.

Earth Resources Observation and Science (EROS) Center. (2020). *Landsat 7 Enhanced Thematic Mapper Plus Level-2, Collection 2 Surface Reflectance*. U.S. Geological Survey. https://doi.org/10.5066/P9C7I13B.

Earth Resources Observation and Science (EROS) Center. (2020). *Landsat 4-5 Thematic Mapper Level-2, Collection 2 Surface Reflectance*. U.S. Geological Survey. https://doi.org/10.5066/P9IAXOVV.

Environmental Mapping Consultants. (2025). [in-situ Coastal Monitoring Stations Data (Unpublished Raw Data). Environmental Mapping Consultants. Retrieved February 4, 2025.

Good, A. M., & Bahr, K. D. (2021). The coral conservation crisis: Interacting local and global stressors reduce reef resiliency and create challenges for conservation solutions. *SN Applied Sciences*, *3*(3). https://doi.org/10.1007/s42452-021-04319-8

Huete, A., Didan, K., Miura, T., Rodriguez, E.P., Gao, X., Ferreira, L.G. (2002). Overview of the radiometric and biophysical performance of the MODIS vegetation indices. *Remote Sensing of Environment,* 83, 195-213. https://doi.org/10.1016/S0034-4257(02)00096-2

Locke, K. A. (2024). Impacts of land use/land cover on water quality: A contemporary review for researchers and policymakers. *Water Quality Research Journal,* 59, 89–106. https://doi.org/10.2166/wqrj.2024.002

NASA Goddard Space Flight Center, Ocean Ecology Laboratory, Ocean Biology Processing Group (2022). *Medium Resolution Imaging Spectrometer (MERIS) ENVISAT MERIS Level-3 Mapped Chlorophyll*, (Version 2022). [Data set]. NASA OB.DAAC. Retrieved February 26, 2025, from https://oceandata.sci.gsfc.nasa.gov/l3/

NASA Goddard Space Flight Center, Ocean Ecology Laboratory, Ocean Biology Processing Group (2022). *Medium Resolution Imaging Spectrometer (MERIS) ENVISAT MERIS Level-3 Mapped Downwelling Diffuse Attenuation Coefficient*, (Version 2022). [Data set]. NASA OB.DAAC. Retrieved February 26, 2025, from https://oceandata.sci.gsfc.nasa.gov/l3/

NASA Goddard Space Flight Center, Ocean Ecology Laboratory, Ocean Biology Processing Group (2024). . *Ocean Color Instrument PACE OCI Level-3 Mapped Chlorophyll,* (V3) [Data set]. NASA OB.DAAC. Retrieved March 5, 2025, from https://oceandata.sci.gsfc.nasa.gov/l3/

NASA Goddard Space Flight Center, Ocean Ecology Laboratory, Ocean Biology Processing Group (2024). *Ocean Color Instrument PACE OCI Level-3 Mapped Downwelling Diffuse Attenuation Coefficient,* (V3) [Data set]. NASA OB.DAAC. Retrieved March 5, 2025, from https://oceandata.sci.gsfc.nasa.gov/l3/

NASA Goddard Space Flight Center, Ocean Ecology Laboratory, Ocean Biology Processing Group (2022). *Visible and Infrared Imager/Radiometer Suite Level-3 Mapped Chlorophyll* (Version 2022). [Data set]. NASA OB.DAAC. Retrieved February 26, 2025, from https://oceandata.sci.gsfc.nasa.gov/l3/

NASA Goddard Space Flight Center, Ocean Ecology Laboratory, Ocean Biology Processing Group (2022). *Visible and Infrared Imager/Radiometer Suite Level-3 Mapped Downwelling Diffuse Attenuation Coefficient,* (Version 2022). [Data set]. NASA OB.DAAC. Retrieved February 26, 2025, from https://oceandata.sci.gsfc.nasa.gov/l3/

NOAA Office for Coastal Management (2017). *2010 C-CAP 30 Meter Land Cover of Puerto Rico*. Retrieved from https://coast.noaa.gov/digitalcoast/data/

O'Reilly, J., Werdell, J., Hu, C., Feng, L., Lee, Z., Franz, B., Bailey, S., Proctor, C. (2023). *Ocean color chlorophyll a algorithm (*Version 1.1). https://doi.org/10.5067/JCQB8QALDOYD

Otero, E., & Carbery, K. K. (2005). Chlorophyll a and turbidity patterns over coral reef systems of La Parguera Natural Reserve, Puerto Rico. *Revista de Biología Tropical*, 53(Suppl 1), 25–32. https://pubmed.ncbi.nlm.nih.gov/17465141/

Protectores de Cuencas. (2017). *Rio Fajardo Watershed Pollution Threat Analysis: Recommend integrated watershed management actions*. Retrieved from https://www.drna.pr.gov/wp-content/uploads/2018/02/R%C3%ADo-Fajardo-WPTA_1%C2%AD_5_Final-compressed.pdf

Ramos-Scharron, C. E., Hernandez, E., Torres-Pulliza, D. (2014). Watershed-and Island wide-scale land cover changes in Puerto Rico (1930s-2004) and their potential effects on coral reef ecosystems. *Science of The Total Environment,* (Vols. 506–507), 241-251. https://doi.org/10.1016/j.scitotenv.2014.11.016

Saeidi, S., Mosallaei, A., Imani Harsini, J., Grósz, J., & Waltner, I. (2023). Assessing the impact of land use and land cover on water quality: A case study of the rákos catchment in Hungary. ARPHA Conference Abstracts, 6, e108160. https://doi.org/10.3897/aca.6.e108160

Seers, B. M., & Shears, N. T. (2015). Spatio-temporal patterns in coastal turbidity – long-term trends and drivers of variation across an estuarine-open coast gradient. *Estuarine, Coastal and Shelf Science*, *154*, 137–151. https://doi.org/10.1016/j.ecss.2014.12.018

Shi, W., & Wang, M. (2010). Characterization of global ocean turbidity from moderate resolution imaging spectroradiometer ocean color observations. *Journal of Geophysical Research: Oceans*, *115*(C11). https://doi.org/10.1029/2010jc006160

U.S. Geological Survey. (2025). *USGS 50071000 Rio Fajardo NR Fajardo, PR.* [Data set]. USGS National Water Data. Retrieved March 4, 2025, from https://waterdata.usgs.gov/monitoring-location/50071000/

U.S. Geological Survey. (2001). *National Land Cover Database Commonwealth of Puerto Rico Land Cover Layer*. Data.gov. Retrieved March 4, 2025, from https://catalog.data.gov/dataset/national-land-cover-database-commonwealth-of-puerto-rico-land-cover-layer

Vijith, H., Dodge-Wan, D. (2020). Applicability of MODIS land cover and Enhanced Vegetation Index (EVI) for the assessment of spatial and temporal changes in strength of vegetation in tropical rainforest region of Borneo. *Remote Sensing Applications: Society and Environment,* 18, 100311. https://doi.org/10.1016/j.rsase.2020.100311

Warren, M. A., Simis, S. G. H., & Selmes, N. (2021). Complementary water quality observations from high and medium resolution Sentinel sensors by aligning chlorophyll-*a* and turbidity algorithms. *Remote Sensing of Environment*, 265, 112651. https://doi.org/10.1016/j.rse.2021.112651

Werdell, J., McKinna, L. (2024). *Ocean color spectral diffuse attenuation coefficient for downwelling irradiance algorithm* (Version 1.0). https://doi.org/10.5067/E6JP5Z1CGRFT

Zhu, Z., Qiu, S., & Ye, S. (2022). Remote Sensing of Land Change: A multifaceted perspective. *Remote Sensing of Environment,* 282(3), 113266. https://doi.org/https://doi.org/10.1016/j.rse.2022.113266

8. Appendices

Appendix A: Marine Water Quality Trendlines

Table A1. *K_d490 trends for the marine water study area between 2002 to 2012.*

K_d490 Trendline Measurements by Marine Subregion					
Subregion	**Measurement**	**Slope**	**P-Value**	**R^2**	**STD Error**
Fajardo Coastline	MERIS (2002-2012)	-0.000001	0.627783	0.002145	0.000002
	VIIRS (2012-2024)	0.000002	0.150375	0.013560	0.000001
Northeast Corridor Coastline	MERIS (2002-2012)	0.0	0.958525	0.000024	0.000001
	VIIRS (2012-2024)	0.0	0.742478	0.000703	0.000001
Vieques Sounds	MERIS (2002-2012)	0.0	0.617159	0.002161	0.000001
	VIIRS (2012-2024)	0.0	0.258013	0.008300	0.0

Table A2. *Chlorophyll-a trend data for the marine water study area between 2002 to 2012.*

Chlorophyll-*a* Trendline Measurements by Marine Subregion					
Subregion	**Measurement**	**Slope**	**P-Value**	**R^2**	**STD Error**
Fajardo Coastline	MERIS (2002-2012)	-0.000061	0.209208	0.015266	0.000049
	VIIRS (2012-2024)	0.000030	0.132896	0.014796	0.000020
Northeast Corridor Coastline	MERIS (2002-2012)	-0.000011	0.694709	0.001393	0.000028
	VIIRS (2012-2024)	0.000001	0.957618	0.000018	0.000011
Vieques Sounds	MERIS (2002-2012)	0.000002	0.831714	0.000391	0.000008
	VIIRS (2012-2024)	-0.000002	0.536659	0.002484	0.000004